Redox Biology 75 (2024) 103241

Contents lists available at ScienceDirect

Redox Biology

journal homepage: www.elsevier.com/locate/redox

Extracellular vesicles from II trimester human amniotic fluid as paracrine conveyors counteracting oxidative stress

Senesi Giorgia [a,b,4], Guerricchio Laura [c,4], Ghelardoni Maddalena [e,1,4], Bertola Nadia [e], Rebellato Stefano [f,g], Grinovero Nicole [h], Bartolucci Martina [h], Costa Ambra [e], Raimondi Andrea [i,2], Grange Cristina [j], Bolis Sara [a], Massa Valentina [k], Paladini Dario [l], Coviello Domenico [m], Pandolfi Assunta [d], Bussolati Benedetta [n], Petretto Andrea [h], Fazio Grazia [f,g], Ravera Silvia [c], Barile Lucio [a,b,**], Balbi Carolina [o,p,***,3,5], Bollini Sveva [c,e,*,5]

[a] Cardiovascular Theranostics, Istituto Cardiocentro Ticino and Laboratories for Traslational Research Ente Ospedaliero Cantonale, CH-6500, Bellinzona, Switzerland
[b] Euler Institute, Faculty of Biomedical Sciences, Università della Svizzera Italiana, CH-6900, Lugano, Switzerland
[c] Department of Experimental Medicine (DIMES), University of Genova, 16132, Genova, Italy
[d] Department of Medical, Oral and Biotechnological Sciences, University "G. d'Annunzio" Chieti-Pescara and Center for Advanced Studies and Technology – CAST, 66100, Chieti, Italy
[e] IRCCS Ospedale Policlinico San Martino, 16132, Genova, Italy
[f] Tettamanti Center, Fondazione IRCCS San Gerardo dei Tintori, 20900, Monza, Italy
[g] School of Medicine and Surgery, University of Milano-Bicocca, 20900, Monza, Italy
[h] Core Facilities – Clinical Proteomics and Metabolomics, IRCCS Istituto Giannina Gaslini, 16147, Genova, Italy
[i] Institute for Research in Biomedicine, Università della Svizzera Italiana, CH-6500, Bellinzona, Switzerland
[j] VEXTRA Facility and Department of Medical Sciences, University of Turin, 10126, Turin, Italy
[k] Department of Health Sciences, University of Milan, 20146, Milan, Italy
[l] Fetal Medicine and Surgery Unit, IRCCS Istituto Giannina Gaslini, 16147, Genova, Italy
[m] Human Genetics Laboratory, IRCCS Istituto Giannina Gaslini, 16147, Genova, Italy
[n] Department of Molecular Biotechnology and Health Sciences, University of Turin, 10126, Turin, Italy
[o] Center for Molecular Cardiology, University of Zurich, 8952, Schlieren, Switzerland
[p] Department of Internal Medicine, Cantonal Hospital Baden, Baden, Switzerland

A R T I C L E I N F O

Keywords:
Extracellular vesicles
Amniotic fluid
Paracrine effect
Oxidative stress
Cell viability
Metabolic dysfunction

A B S T R A C T

Background: We previously demonstrated that the human amniotic fluid (hAF) from II trimester of gestation is a feasible source of stromal progenitors (human amniotic fluid stem cells, hAFSC), with significant paracrine potential for regenerative medicine. Extracellular vesicles (EVs) separated and concentrated from hAFSC secretome can deliver pro-survival, proliferative, anti-fibrotic and cardioprotective effects in preclinical models of skeletal and cardiac muscle injury. While hAFSC-EVs isolation can be significantly influenced by in vitro cell culture, here we profiled EVs directly concentrated from hAF as an alternative option and investigated their paracrine potential against oxidative stress.
Methods: II trimester hAF samples were obtained as leftover material from prenatal diagnostic amniocentesis following written informed consent. EVs were separated by size exclusion chromatography and concentrated by ultracentrifugation. hAF-EVs were assessed by nanoparticle tracking analysis, transmission electron microscopy,

* Corresponding author. Dept. Experimental Medicine (DIMES), Largo R. Benzi 10, 16132, Genova, Italy.
** Corresponding author. Istituto Cardiocentro Ticino and Laboratories for Translation Research, EOC, CH-6500, Bellinzona, Switzerland.
*** Corresponding author. Center for Molecular Cardiology, University of Zurich, Zurich, Switzerland.
E-mail addresses: lucio.barile@eoc.ch (B. Lucio), carolina.balbi@uzh.ch (B. Carolina), sveva.bollini@unige.it (B. Sveva).
[1] Ghelardoni M.: Department of Medical, Oral and Biotechnological Sciences, University "G. d'Annunzio" and Center for Advanced Studies and Technology – CAST, 66100 Chieti, Italy.
[2] Raimondi A.: Experimental Imaging Centre, IRCCS Istituto Scientifico San Raffaele, 20132 Milan, Italy.
[3] Balbi C.: Cardiovascular Theranostics, Istituto Cardiocentro Ticino and Laboratories for Traslational Research Ente Ospedaliero Cantonale, 6500 Bellinzona, Switzerland.
[4] Equal contribution as first authorship.
[5] Equal contribution as senior authorship.

https://doi.org/10.1016/j.redox.2024.103241
Received 20 April 2024; Received in revised form 7 June 2024; Accepted 15 June 2024
Available online 17 June 2024

Western Blot, and flow cytometry; their metabolic activity was evaluated by oximetric and luminometric analyses and their cargo profiled by proteomics and RNA sequencing. hAF-EV paracrine potential was tested in preclinical in vitro models of oxidative stress and dysfunction on murine C2C12 cells and on 3D human cardiac microtissue.

Results: Our protocol resulted in a yield of $6.31 \pm 0.98 \times 10^9$ EVs particles per hAF milliliter showing round cup-shaped morphology and 209.63 ± 6.10 nm average size, with relevant expression of CD81, CD63 and CD9 tetraspanin markers. hAF-EVs were enriched in CD133/1, CD326, CD24, CD29, and SSEA4 and able to produce ATP by oxygen consumption. While oxidative stress significantly reduced C2C12 survival, hAF-EV priming resulted in significant rescue of cell viability, with notable recovery of ATP synthesis and concomitant reduction of cell damage and lipid peroxidation activity. 3D human cardiac microtissues treated with hAF-EVs and experiencing H_2O_2 stress and TGFβ stimulation showed improved survival with a remarkable decrease in the onset of fibrosis.

Conclusions: Our results suggest that leftover samples of II trimester human amniotic fluid can represent a feasible source of EVs to counteract oxidative damage on target cells, thus offering a novel candidate therapeutic option to counteract skeletal and cardiac muscle injury.

1. Background

Perinatal derivatives from extra-embryonic tissue are attracting increasing interest due to their regenerative potential against a variety of diseases. Mesenchymal stromal cells (MSC) from perinatal clinical waste (III trimester placenta membranes, umbilical cord, and amniotic fluid) or from leftover samples of prenatal screening (II trimester amniotic fluid from amniocentesis) have been proposed as alternatives over adult progenitors given their modulatory profile and high self-renewal capacity [1–3]. Moreover, being perinatal derivatives developmentally more immature, they have not been exposed to a lifetime of environmental stimuli (i.e. *inflammaging*) that may negatively affect their biological profile; besides, recent reports from preclinical and clinical studies suggest that they are safe and effective.

The human amniotic fluid (hAF) represents an easily exploitable source of progenitor cells which can be collected along pregnancy following amniocentesis procedures (as fetal human amniotic fluid-derived stem cells, hAFSC) or at term during scheduled C-section delivery (as perinatal hAFSC). hAFSC have shown remarkable paracrine potential in promoting tissue regeneration in several models of inflammatory-based or ischemic disease [4–9]. Functional assays by our group and others indicated that extracellular vesicles (EVs) secreted by hAFSC (hAFSC-EVs) act as major conveyors of pro-survival, cardioprotective, neurotrophic, anti-inflammatory, and anti-fibrotic effects in different preclinical studies [7,8,10–19]. EVs are membrane-bound nanoparticles with heterogeneous size distribution (from 50- up to 1000 nm) released by all cells; they act as mediators of intercellular signalling via the horizontal transfer to responder cells of their cargo enriched in bioactive molecules. As a matter of fact, MSC-EVs play pivotal roles in orchestrating different biological processes, including the modulation of the immune response and the activation of pro-resolving mechanisms driving tissue repair [20]. Since the EV content mirrors the paracrine profile of the parental cell, preconditioning strategies have been optimised to prime progenitor cells to enhance their regenerative potential. When stimulated in vitro by a short burst of hypoxia, hAFSC demonstrated to secrete EVs endowed with significant cardio-active profile [7,8,12]. Nevertheless, standardisation of the manufacturing of the hAFSC secretome, including EVs, is currently a matter of optimization. Therefore, here we investigated whether the II trimester hAF can represent an alternative appealing source of EVs with paracrine activity similar to hAFSC-EVs, thus offering an effortless and less time-consuming option for biotech and translational purposes.

The biological activity of hAF-EVs has been recently evaluated in preclinical models of murine neonatal hypoxic encephalopathy with relevant improvement of local angiogenesis [21], in inflammatory-related models with quenching of the T cell immune response [22] and in terms of modulation of the inflammasome activation in human monocytes [23]. Notably, a cell-free biological formulation of human term amniotic fluid enriched in EVs has been recently reported to significantly decrease inflammatory cytokine production in preclinical murine models of SARS-CoV-2 infection in vitro and *in vivo* [24]. Nevertheless, these promising results have been documented for III trimester hAF-EVs from clinical waste samples obtained by elective C-section procedures; currently, very little is known about the pro-resolving and regenerative capacity of more immature II trimester hAF-EVs.

Therefore, here we (i) validated a straightforward protocol to efficiently separate and concentrate EVs from leftover samples of II trimester hAF obtained during routine prenatal screening; (ii) provide their phenotypic characterization, and (iii) profile their paracrine potential in counteracting oxidative stress on responder cells and in restraining pro-fibrotic activation in vitro, two hallmarks of skeletal muscle and cardiac dysfunction with relevant clinical impact.

2. Material and methods

2.1. hAF-EVs separation and concentration

II trimester human amniotic fluid (hAF) samples were collected as leftover material via amniocentesis for routine prenatal screening donated for research purposes by healthy donors at IRCCS Istituto G. Gaslini in Genova, Italy. All patients provided informed written consent in accordance with specific authorization (P.R. 428REG2015 from *Comitato Etico Regione Liguria*) and in compliance with Helsinki Declaration ethical principles. hAF samples were obtained from 36.48 ± 0.64-year-old female healthy donors (n = 33 in total, with no prior history of oncological and/or infective diseases, including HIV and hepatitis infections) as validated for unaltered karyotype. hAF samples (4.33 ± 0.18 mL average volume) were subjected to centrifugation at 300×*g* for 5 min at room temperature to isolate cellular content. The supernatant was then further processed at 300×*g* for 10 min and then at 2000×*g* for 20 min at 4 °C to remove any remaining cellular debris. The supernatant was subsequently concentrated by means of ultrafiltration using 100 kDa selective cut-off membranes, according to manufacturer's instructions (Amicon Ultra-15 Centrifugal Filter, Merck Millipore) up to a final volume of 1 mL. The concentrated samples were stored at −80 °C until use. Size exclusion chromatography (SEC) was employed to isolate hAF-EVs by using IZON qEV original 70 nm columns (Izon Science). In accordance with manufacturer's guidelines, 1 mL of hAF was loaded onto the column and eluted with 1X Phosphate-buffered saline (PBS) solution. The hAF-EVs-enriched fractions were collected and concentrated by ultracentrifugation (UC) at 100,000×*g* for 120 min in an ultracentrifuge (Beckman Coulter Optima XPN-100; Beckman Coulter) with SW55Ti swinging bucket rotor. EV samples were then resuspended in sterile PBS solution for following analyses.

2.2. Characterization of hAF-EVs

hAF-EV size distribution and yield were determined by Nanoparticle Tracking Analysis (NTA, Nanosight NS300, Malvern Panalytical). Samples were acquired and recorded under a controlled continuous flow at 25 °C. For each measurement, 5 videos of 60 s were captured. Samples were characterised using NTA 3.2 software with a detection threshold equal to 5 as the ratio of total completed tracks over total valid tracks. EV morphological evaluation was performed by transmission electron microscopy (TEM) negative staining. hAF-EV samples were absorbed on a glow-discharged carbon-coated formvar copper grid and negatively stained with 2 % uranyl acetate. EV pictures were examined by a Talos L120C operating at 120 kV. Images were acquired with a Ceta CCD camera (all FEI, Thermo Fisher Scientific). Dimension distribution analysis was performed using ImageJ software (https://imagej.download.it/). Canonical expression of EV markers was analysed by Western Blot (WB) and flow cytometry. Samples were prepared following two different protocols, according to the specific marker to be evaluated. To define TSG101, Syntenin-1, ALIX and APO-B48 expression, hAF-EV and hAF samples were boiled at 95 °C with Laemmli SDS sample buffer 6X (VWR International, Dietikon), for 10 min; for CD63 and CD81 expression, hAF-EVs and hAF samples were mixed with Laemmli sample buffer 6X without SDS. Samples were then separated on 4–20 % Mini-PROTEANTGXTM Precast Gel, and transferred onto a PVDF membrane with a semi-dry transfer system (all from Bio-Rad Europe). Membranes were incubated with the following primary antibodies: anti-TSG101 (1:1000 ab125011); anti-Syntenin-1 (1:1000 ab19903); anti-ALIX (1:1000 ab186429); anti-APO-B48 (1:500 ab20737, all from Abcam); anti-CD63 (1:1000, 10628D, Invitrogen) and anti-CD81 (1:1000, 555675, Becton-Dickinson, BD). IRDye 680RD- or 800CW- goat anti-mouse or goat anti-rabbit secondary antibodies were then used (LI-COR Biosciences, LicorBio). Infrared signal was detected using an Odyssey CLx Detection System (LI-COR Biosciences). Concentrated hAF samples were used as comparative reference. CD9, CD63 and CD81 (JSR Life Science) expression was also investigated by flow cytometry (FC) as previously described [25]. 1×10^{10} hAF-EVs resuspended in 100 μL of PBS1X were incubated overnight at 10 °C and 400 rpm with 1 μL of CD9, CD63, and CD81 (JSR Life Sciences Ex-C9-SP; Ex-C63-SP; Ex-C81-SP; ratio 1:1:1) mixed beads, corresponding to 1.2×10^5 beads in total (for each test). After 24 h, 1 μL of 10 μg/mL of FITC-conjufigated CD9 (Biolegend 312104) or 10 μg/mL of PE-conjugated CD63 (Biolegend 353004) or 5 μg/mL of PE-conjugated CD81 (Biolegend 349505) was added to 100 μL of hAF-EVs and bead-containing samples, which were then acquired (20000 events) with CytoFLEX (Beckman Coulter) and analysed using Kaluza software (Beckman Coulter). hAF-EVs samples underwent bead-based EVs immunocapture and were analysed by MACSPlex human Exosome Kit (Miltenyi Biotec), according to previously validated studies [26,27]; hAF-EVs were incubated with 37 fluorescently labelled capture bead populations, each coated with a specific antibody binding the respective surface epitope, and 2 control bead populations, followed by EVs detection reagent (i.e. fluorescently labelled antibodies for the canonical CD9/CD63/CD81 tetraspanin markers). Median fluorescence intensity (MFI) was measured on a MACSQuantAnalyzer10 flow cytometer (Miltenyi Biotec). All markers were analysed simultaneously. Surface epitope levels were referenced to EV-specific epitopes by subtracting the respective fluorescence values of blank control from MFI values for individual epitopes and normalizing them for CD9/CD63/CD81 MFI, reflecting EV concentration. Super-resolution microscopy was performed on a Nanoimager S Mark II microscope from ONI (Oxford Nanoimaging) using the EV profiler Kit (ONI) according to the manufacturer's protocol. The microscope was equipped with a 100x, 1.4NA oil immersion objective, an XYZ closed-loop piezo 736 stage, and triple emission channels split at 640, 488 and 555 nm. For EV characterization, the EV profiler Kit (ONI) was used following manufacturer's protocol. The Kit contains anti CD9-488, CD63-568 and CD81-647 fluorescent antibodies and all the buffers and reagents necessary for the experiment. The CD81-647 antibody was substituted with the anti-human HLA-G one conjugated with APC (Miltenyi Biotec). Images were performed in dSTORM mode and acquired sequentially in total reflection fluorescence (TIRF) mode. Single-molecule data was filtered using NimOS software (v.1.18.3, ONI). Data has been analysed with the Collaborative Discovery (CODI) online analysis platform (www.alto.codi.bio from ONI) and the drift correction pipeline version 0.2.3 was used [28].

2.3. Molecular profiling of hAF-EVs cargo

hAF-EVs samples were lysed and proteins denatured, reduced, and alkylated with 50 μL of iST-LYSE buffer (PreOmics) for 10 min at 95 °C on an Eppendorf ThermoMixer at 1000 rpm. Protein concentration in lysed samples was assessed by tryptophan fluorescence emission assay and 8 μg of protein lysates were used for subsequent analyses. Protein Aggregation Capture (PAC)-based protein isolation and digestion were performed on a KingFisher™ Apex magnetic handling station (Thermo Scientific) in a 96-well format. More in detail, 1:1 Sera-Mag™ Speed-Bead Carboxylate Modified Magnetic Particles 45152105050250 and 65152105050250 (Cytiva) were added to lysed samples in plate #1 with a protein/bead ratio of 1:4 (w/w). 70 % ACN (v/v) was used to induce protein aggregation. After mixing, the solution was allowed to settle to precipitate proteins on beads (two cycles of 1 min of mixing at medium speed, followed by a 10 min pause each). Sequential washes with 100 % ACN (x3), 70 % ethanol and isopropanol (plates #2–6) were performed for 2.5 min at slow speed, without releasing the beads from the magnet. The captured proteins were then digested in 100 μL of 25 mM Tris, pH 8, with 0.7 μg trypsin (Promega) and 0.3 μg Lys-C (Wako) for 2.5 h at 37 °C in plate #7. Once the process was completed, the magnetic beads were removed from the digested samples and placed back into plate #1. Peptide mixtures were acidified using 2 % trifluoroacetic acid (TFA) to quench protease activity and desalted according to the in-StageTip (iST) method [29]. Eluted peptides were dried by vacuum centrifugation and resuspended in 2 % ACN, 0.1 % formic acid (FA) in water. Peptides were separated on an EASY-Spray PepMap RSLC C18 column (50 cm × 75 μm, 2 μm particle size, Thermo Scientific) using a 50 min gradient ranging from 2 % solution B (80 % ACN, 5 % dimethyl sulfoxide (DMSO), and 0.1 % FA) to 45 % B at a flow rate of 250 nL/min. The mass spectrometer was operated in positive polarity and data-independent acquisition (DIA) mode. Full scans (m/z 375–1500) were acquired in the Orbitrap at 70,000 resolution with the automatic gain control (AGC) target set to 3 × 106. Precursors were selected for data-independent fragmentation with an isolation window width of 34 m/z and 19 loop count. The higher collisional dissociation energy for MS/MS fragmentation was set to 27 %. MS2 scans were acquired at 35,000 resolution with 3 × 106 AGC target. Raw files were analysed by Spectronaut v18 (Biognosys AG) using a library-free approach (directDIA) under default settings. Enzymes/Cleavage Rules were set to Trypsin/P, LysC. The library was generated against the Uniprot Human database (release UP000005640_9606, November 2022). Carbamidomethylation was selected as a fixed modification, while methionine oxidation and N-terminal acetylation were selected as variable modifications. The false discovery rate (FDR) of peptide spectrum match (PSM) and peptide/-protein groups was set to 0.01. For quantification, Precursor Filtering was set to Identified (Qvalue) and MS2 was chosen as quantity MS-level. Raw files were processed by Spectronaut v18 (Biognosys AG) using the directDIA search against the UniProt Human database (release UP000005640_9606, November 2022) under default settings.

Oximetric and luminometric analyses were performed on hAF-EVs permeabilized by 0.03 % digitonin. Oxygen consumption rate (OCR) was assayed by a thermostatically controlled oxygraph apparatus equipped with an amperometric electrode. ATP synthesis through FoF1-ATP synthase (ATP synthase) was evaluated by a luminometer, employing the luciferin/luciferase chemiluminescent method in the presence of the following solutions: 0.1 mM ADP, 0.6 mM ouabain, 0.25

mM di(adenosine)-5-penta-phosphate (an adenylate kinase inhibitor) [30]. Oxidative phosphorylation (OxPhos) efficiency was assessed by means of calculating the ratio between synthesized ATP and OCR (P/O value). In the presence of succinate as respiratory substrates, the P/O ratio around 1.5 indicates that ATP production and oxygen consumption are coupled, thus minimizing the reactive oxygen species (ROS) production. hAF-EVs samples were processed by QIAzol™ Lysis Reagent (Qiagen) suspension and RNA extraction was performed with miRNeasy Micro Kit (Qiagen). Whole-transcriptome RNA-sequencing (RNAseq) analysis was performed by Next-Generation Sequencing, using the Universal Plus™ Total RNAseq library preparation kit with NuQuant® with targeted transcript depletion with AnyDeplete (Tecan) for globin genes. The yields of final libraries were assessed by Qubit 4.0 fluorimeter, and their sizes were measured by 2100 Agilent Bioanalyzer (Agilent). The libraries were analysed by paired-end sequencing on NextSeq550 Illumina platform, 2 × 75bp. FASTQ files are available in the ArrayExpress database (www.ebi.ac.uk/arrayexpress) under accession number E-MTAB-14034. Raw FASTQ sequences were processed with DRAGEN RNA v4.0.4 pipeline (Illumina) and genes quantification files were extracted. The comparison of individual gene expression levels used TPMs (Transcripts Per Million) as the measurement unit. A median value was computed for each gene across samples, and genes with expression levels below 1 TPM were excluded due to their potential as artifacts. The average of all gene medians was then calculated, and genes exhibiting a median expression higher than this threshold were selected for the enrichment analysis, which was performed through the freely available Enrichr tool (https://maayanlab.cloud/Enrichr/).

2.4. Analysis of hAF-EV paracrine potential in vitro

2.4.1. Cell culture

The mouse myoblast C2C12 cell line was purchased from Interlab Cell Line Collection (ICLC) and cultured at 37 °C and 5 % CO2 in high glucose Dulbecco's Modified Essential Medium (DMEM) medium with 10 % FBS, 2 % L-glutamine and 1 % penicillin/streptomycin (all EuroClone), as previously described [7]. Human 3D microtissue (hMT) was generated from human induced pluripotent cell (iPS)-derived cardiomyocytes (hCM), human cardiac fibroblast (hCF), and human aortic endothelial cells (hAEC) according to Ref. [31]. Briefly, hCM were obtained differentiating iPS cells as previously described [11]. hCF were derived from enzymatic digestion of leftover cardiac atrial appendage tissue samples obtained from patients with no significant coronary artery disease, undergoing heart surgery for aortic regurgitation. Cardiac tissue was donated for research purposes at Istituto Cardiocentro Ticino-EOC, Switzerland. All patients provided informed written consent in accordance with specific authorization (*Comitato Etico Cantonale*, Bellinzona, Switzerland; Ref.CE 2923) and in compliance with Helsinki Declaration ethical principles. hCF were obtained following enzymatic dissociation of the atrial specimens. Briefly, atrial specimens were minced and incubated for 45 min at 37 °C with a APS1X buffer containing 1 mg/mL Liberase™ (Roche). Obtained cells were cultured in EGM-2 complete medium, composed by EBMTM-2 Basal Medium and EGM TM-2 Single QuotsTM Supplements (CC-3156, Lonza). Lastly, hAEC were purchased from Lonza (CC-2535, Lonza) and cultured in EGM-2 complete medium supplemented with 10 % FBS. Human 3D microtissue (hMT), were obtained combining hCM, hCF and hAEC in the proportion of 1:0.2:0.2 (3500:750:750 cells) using low-binding BIOFLOAT™ 96-well plates (faCellitate). After a centrifugation at 1100 rpm for 5 min, hMT were further maintained in vitro in EGM-2 complete medium. Two days after plating hMT were spontaneously beating and used in vitro.

2.4.2. Preclinical models of oxidative stress

hAF-EVs pro-survival paracrine potential was evaluated on C2C12 cells undergoing 1 μM H_2O_2 oxidative stress. C2C12 were primed with 5 × 10^7 hAF-EVs particles/ml under serum-free conditions for 3 h. Oxidative stress and cellular damage were subsequently induced by administering 1 μM H_2O_2 for 2 h. Cells were then cultured in complete medium for 20 h. Cell viability was then assessed by 3-(4,5-dimethylthiazol-2-yl)-2,5-diphenyltetrazolium bromide (MTT) assay using a 0.5 mg/mL MTT solution (Sigma-Aldrich) and absorbance read at 570 nm on a Biotek ELx808 Absorbance Microplate Reader with Biotek Gen5 2.03 software. Energy metabolism and oxidative damage accumulation were also evaluated on C2C12 cells in control conditions and undergoing oxidative stress with or without EV priming by assaying the aerobic ATP synthesis, the OCR, the lactate dehydrogenase (LDH) activity, and the malondialdehyde (MDA) concentration. The activity of ATP synthase was evaluated on 1 × 10^5 cells resuspended in PBS with 0.6 mM ouabain and 0.25 mM di(adenosine)-5-Penta-phosphate, and permeabilized with 0.03 mg/mL digitonin. The reaction was monitored with a luminometer employing the luciferin/luciferase chemiluminescent method, stimulating the cells with 10 mM pyruvate, 5 mM malate, and 0.1 mM ADP. OCR activity was measured on 1 × 10^5 digitonin-permeabilized cells resuspended in PBS by an amperometric electrode in a closed chamber, using 10 mM pyruvate and 5 mM malate as respiratory substrate. As for hAF-EVs, OxPhos efficiency was analysed by P/O value; in the presence of pyruvate plus malate, P/O ratio should be around 2.5 with energy production and respiration being coupled. Lactate dehydrogenase (EC 1.1.1.27) activity was assayed spectrophotometrically at 340 nm, following the NADH oxidation. The assay medium contained: 100 mM Tris–HCl pH 7.4, 0.2 mM NADH, and 5 mM pyruvate. MDA concentration was evaluated by the thiobarbituric acid reactive substance (TBARS) assay [32]. The TBARS solution was composed of 0.25 M HCl, 0.25 mM trichloroacetic acid, and 26 mM thiobarbituric acid. An amount of 50 μg of cell homogenate protein dissolved in 300 μL of Milli-Q water was added along with 600 μL of TBARS solution. For 1 h, the mixture was incubated at 95 °C and evaluated spectrophotometrically at 532 nm. MDA standard solutions with concentrations between 1 and 20 μM were employed for the calibration. hMT were pre-treated with 1 × 10^7 hAF-EVs/hMT for 3 h before exposing them to 1 mM H_2O_2 for 2 h hMT were then cultured in complete EGM2 medium for 24 h and analysed by CCK8 assay (Dojindo, Tabaru as per manufacturer's instructions).

To induce ROS production, hCF were treated with 10 ng/mL TGFβ1 (CYT-716, Prospect) for 3 h and then incubated with 1 μg/mL of dihydroethidium (DHE, Thermo Fisher Scientific) for 30 min at 37 °C. Live cells were then counterstained with Hoechst 33342 (1 μg/mL - Thermo Fisher Scientific). Images were acquired with Lionheart FX automated microscopy and analysed with Gen5 software (Biotek) to evaluate DHE mean fluorescent signal. To induce the pro-fibrotic activation of hCF into myofibroblasts, hMT were treated with 10 ng/mL TGFβ1 (CYT-716, Prospect) after being primed with 1 × 10^7 hAF-EVs/hMT and analysed after 7 days. hMT dimension was evaluated by bright field pictures. Images were acquired with Lionheart FX automated microscopy and analysed with Gen5 software (Biotek).

2.4.3. Uptake of hAF-EVs from target cells

hAF samples (500 μL) were labelled with 5 μL of the commercially available lipophilic near-infrared fluorescent cyanine dye DiR (2.5 mg/mL; Thermo Fisher Scientific) and incubated at 37 °C for 5 min under gentle shaking. hAF-EVs were then separated by SEC, thus helping eliminate the unbound dye in excess, and concentrated by UC, as described above in paragraph 2.1. C2C12 cells and hMT were incubated under serum-free conditions with DiR-labelled hAF-EVs and live images were acquired 24 h later using the automated microscope BioTek Lionheart FX (Biotek); acquisition was performed within a heated chamber (37 °C).

2.4.4. Biochemical and molecular analyses of target cells

hMT were fixed with 4 % PFA solution for 5 min at room temperature (RT). hMT were then permeabilized with 0.3 % Triton X (Triton X detergent, Sigma-Aldrich) and blocked in 2 % bovine serum albumin

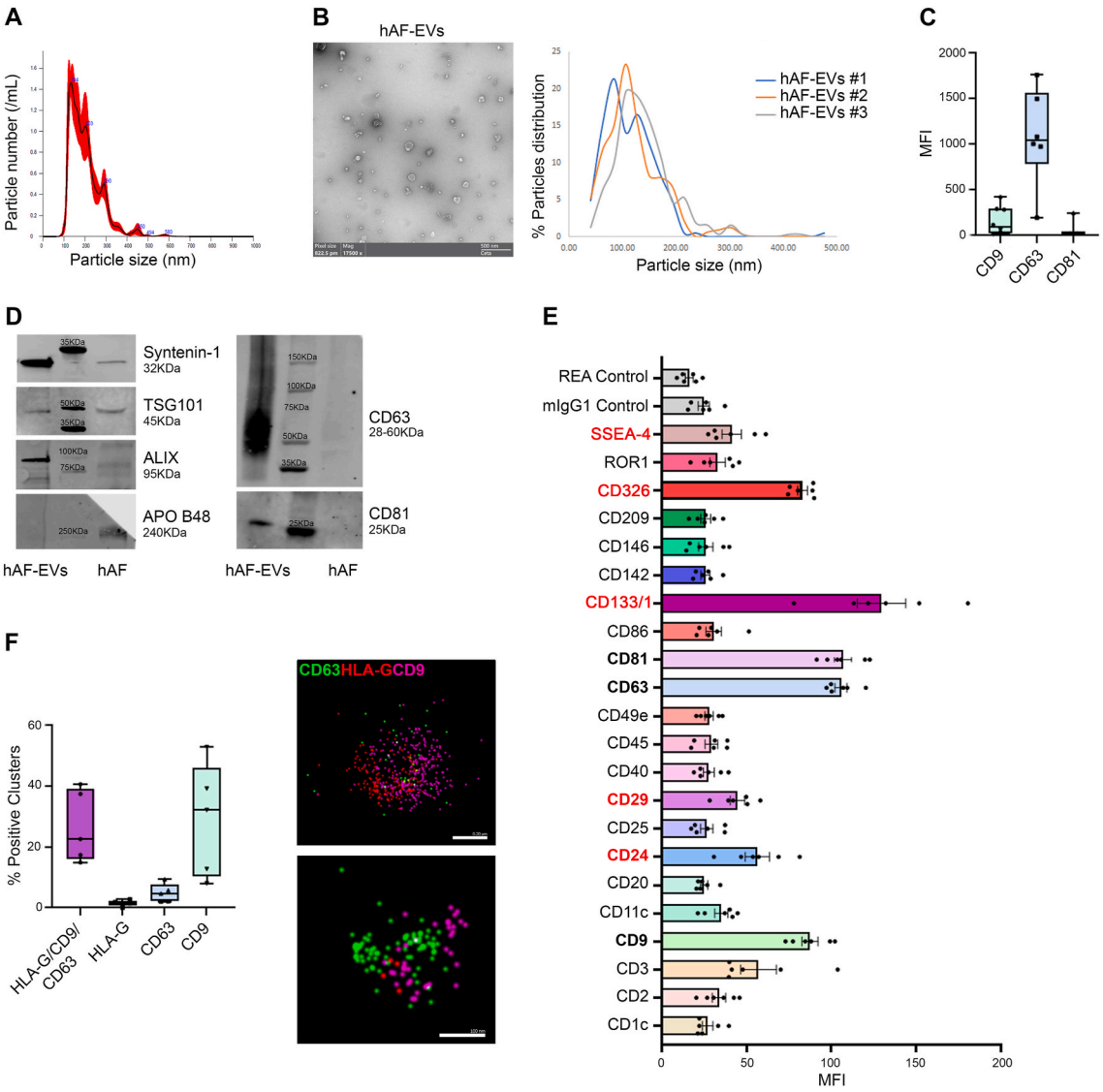

Fig. 1. Characterization of hAF-EVs. A) Representative graphical output of hAF-EVs size distribution by nanoparticle tracking analysis; **B)** hAF-EVs morphology and ultrastructure analysis by TEM with representative image of hAF-EVs and evaluation of the particle distribution according to size (n = 3); scale bar: 500 nm; **C)** Flow cytometry analysis of hAF-EVs for the expression of the CD9, CD63 and CD81 tetraspanin antigens; graph shows the mean ± s.e.m value referring to each antigen expression MFI (n = 4); **D)** Representative cropped images of Western Blot analyses of hAF-EVs and hAF for the expression of the canonical EV markers Syntenin-1, TSG101, ALIX, CD81 and CD63 and for APO B48 as lipoprotein marker (n = 4); **E)** Immunophenotyping of hAF-EVs by flow cytometry and MacsPlex Assay for surface antigens profiling; the graph shows the mean ± s.e.m value referring to each antigen expression MFI (n = 6); **F)** Super-resolution microscopy analysis on hAF-EV for the expression of CD9, CD63 and HLA-G; the graph on the left shows the mean ± s.e.m value referring to the percentage of clusters positive for: triple expression of HLA-G, CD9 and CD63 and single expression of HLA-G or CD63 or CD9 (n = 5); representative images on the right represent single hAF-EV expressing CD63 (green), HLA-G (red), CD9 (magenta), scale bar: 200 and 100 nm. (For interpretation of the references to colour in this figure legend, the reader is referred to the Web version of this article.)

(BSA, Merck) in PBS for 40 min at RT, followed by a 5 min wash with PBS. hMT were incubated for two days at RT under slow agitation with the following primary antibodies: Cardiac Troponin T for hCM (cTnT, 1:300, 564766, BD Biosciences); Vimentin for hCF (1:500, ab92547, Abcam); and Cleaved-Caspase 3 (C-Casp3, 1:1000, Cell Signaling). hMT were then incubated with fluorophore-conjugated secondary antibodies for 24 h at RT (Alexa Fluor-488; Alexa Fluor-594 and Alexa Fluor-633, 1:400, Thermo Fisher Scientific) then included for imaging into chamber slide in 1 % low melt Agarose (H26417-14, Thermo Fisher Scientific). Samples were imaged on the Stellaris 5 Confocal Microscope (Leica) at 20X magnification and processed with ImageJ (https://imagej.download.it/) software. Same threshold was used for all the samples.

Total RNA from hMT was obtained using TRIzol™ (Thermo Fisher Scientific) following manufacturer's instructions. Obtained RNA was further transcribed into cDNA using GoScript™ Reverse Transcription System (Promega Madison) as for manufacturer's instructions. Real time qRT-PCR was then performed on a CFX Connect™ Real-Time PCR Detection System (Bio-Rad). Fold change of Collagen I (COLL-I) gene expression was evaluated by $2^{-\Delta\Delta Ct}$ method, considering human GAPDH as housekeeping reference and hMT in control conditions as calibrator. Primer sequences were the following: human COLL-I Forward: AGTGGTTTGGATGGTGCCAA Reverse: GCACCATCATTTCCACGAGC; human GAPDH forward: TGCACCACCAACTGCTTAGC Reverse: GCATGGACTGTGGTCATGAG.

2.5. Statistical analyses

Results are presented as mean with standard error of the mean (s.e.

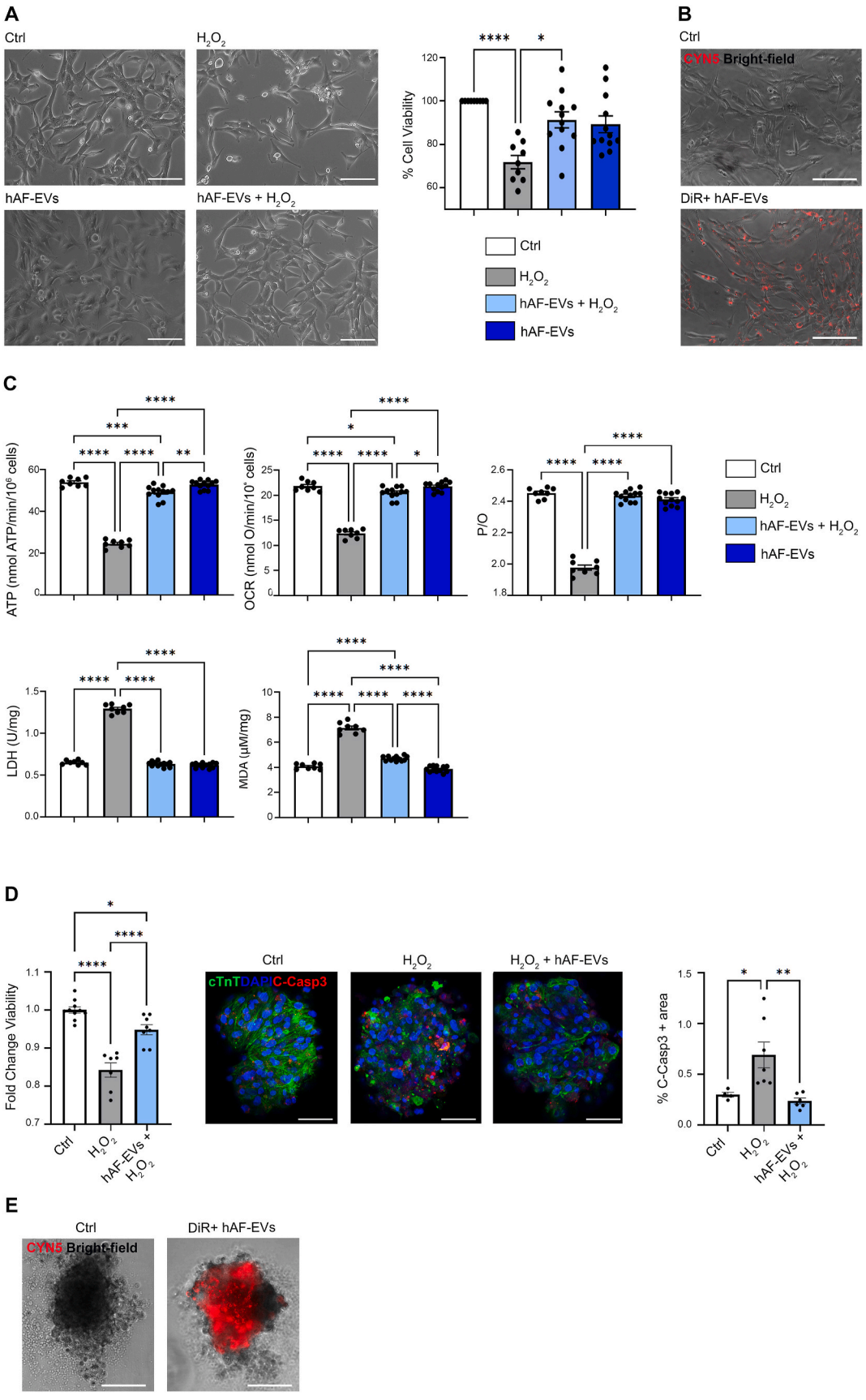

(caption on next page)

Fig. 2. hAF-EV paracrine potential against oxidative stress from H_2O_2 injury. A) On the left: representative images of C2C12 cells under control conditions (*Ctrl*); after 2 h exposure to 1 μM H_2O_2 (*H_2O_2*), following 3 h treatment with hAF-EVs (*hAF-EVs*) and after being primed with hAF-EVs for 3 h and exposed to 1 μM H_2O_2 for 2 h (*hAF-EVs* + *H_2O_2*), scale bar: 200 μm. On the right: graph showing the mean ± s.e.m value referring to C2C12 viability with and without oxidative stress and hAF-EV priming by MTT assay (*Ctrl*: 100 %, n = 9; *H_2O_2*: 71.80 ± 3.10 %, n = 9; *hAF-EVs* + *H_2O_2*: 91.30 ± 3.71 %, n = 12; *hAF-EVs*: 89.30 ± 3.90 %, n = 12; ****p < 0.0001; *p = 0.0228 *H_2O_2* versus *hAF-EVs* + *H_2O_2*). **B)** Representative images of hAF-EV uptake from target C2C12 cells in vitro; images were obtained on live cells visualized by means of phase contrast microscopy (*Bright-field*) while DiR + hAF-EVs were in red (*CYN5*); scale bar: 200 μm. **C)** Metabolic profile of C2C12 with and without oxidative stress (n = 8) and with hAF-EV priming (n = 12). The graphs show the mean ± s.e.m value of the following analyses: ATP synthesis by nmol ATP/min/10^6 cells (*Ctrl*: 53.91 ± 0.70; *H_2O_2*: 24.54 ± 0.70; *hAF-EVs* + *H_2O_2*: 49.15 ± 0.90; *hAF-EVs*: 52.80 ± 0.61; ****p < 0.0001; ***p = 0.0005 *Ctrl* versus *hAF-EVs* + *H_2O_2*; **p = 0.0032 hAF-*EVs* + *H_2O_2* versus *hAF-EVs*, *nmol: nanomoles, min: minutes)*; oxygen consumption rate (OCR) by nmol O/min/10^6 cells (*Ctrl*: 21.81 ± 0.34; *H_2O_2*: 12.41 ± 0.31; *hAF-EVs* + *H_2O_2*: 19.70 ± 0.92; *hAF-EVs*: 21.75 ± 0.30; ****p < 0.0001; *p = 0.0382 and p = 0.0241 for *Ctrl* versus *hAF-EVs* + *H_2O_2 and hAF-EVs* + *H_2O_2* versus *hAF-EVs*, respectively; *O: oxygen*) and P/O ratio (*Ctrl*: 2.45 ± 0.01; *H_2O_2*: 1.98 ± 0.01; *hAF-EVs* + *H_2O_2*: 2.41 ± 0.01; *hAF-EVs*: 2.43 ± 0.01; ****p < 0.0001); LDH activity by U/mg (*Ctrl*: 0.65 ± 0.01; *H_2O_2*: 1.30 ± 0.02; *hAF-EVs* + *H_2O_2*: 0.63 ± 0.01; *hAF-EVs*: 0.62 ± 0.01; ****p < 0.0001; *U: units; mg: milligrams)* and MDA activity by μM/mg (*Ctrl*: 4.10 ± 0.08; *H_2O_2*: 7.15 ± 0.15; *hAF-EVs* + *H_2O_2*: 4.71 ± 0.07; *hAF-EVs*: 3.86 ± 0.08; ****p < 0.0001; *μM: micromolar; U: units; mg: milligrams)*. **D**) Viability analysis on hMT under control conditions (*Ctrl*), after 2 h exposure to 1 mM H_2O_2 (*H_2O_2*), following 3 h treatment with hAF-EVs (*hAF-EVs*) and after being primed with hAF-EVs for 3 h and exposed to 1 mM H_2O_2 for 2 h (*hAF-EVs* + *H_2O_2*). The graph on the left refers to the CCK8 viability assay showing the mean ± s.e.m value referring to hMT viability in fold change with and without oxidative stress and hAF-EVs priming (n = 7; *Ctrl*: 1.00 ± 0.01; *H_2O_2*: 0.84 ± 0.02; *hAF-EVs* + *H_2O_2*: 0.95 ± 0.01; ****p < 0.0001; *p = 0.0217). Panel on the right refers to cleaved Caspase-3 expression (C-Casp3) by hMT under control conditions (*Ctrl*), after 2 h exposure to 1 mM H_2O_2 (*H_2O_2*), following 3 h treatment with hAF-EVs (*hAF-EVs*) and after being primed with hAF-EVs for 3 h and exposed to 1 mM H_2O_2 for 2 h (*hAF-EVs* + *H_2O_2*) with representative images of immunohistochemical staining for cTnT-positive cardiomyocytes (green) and apoptotic C-Casp3-positive cells (red); nuclei are in blue by DAPI; scale bar: 50 μm. On the right graph showing mean ± s.e.m value of C-Casp3 area in percentage (*Ctrl*: 0.30 ± 0.02 %, n = 4; *H_2O_2*: 0.70 ± 0.13 %, n = 7; *hAF-EVs* + *H_2O_2*: 0.24 ± 0.03 %, n = 6; *p = 0.0374; **p = 0.0074); **E)** Representative images of hAF-EV uptake from hMT in vitro; images were obtained on live hMT visualized by phase contrast microscopy (*Bright-field*) while DiR + hAF-EVs were in red (*CYN5*); scal bar: 200 μm. (For interpretation of the references to colour in this figure legend, the reader is referred to the Web version of this article.)

m) of at least three (n = 3) independent experiments as technical (C2C12 cell line) and biological (hAF-EVs, hMT and hCF) replicates. hAF-EV samples were tested as independent preparations, each obtained from a corresponding independent donor. According to normality analysis, comparisons were drawn by one-way ANOVA followed by post-hoc Tukey's multiple comparisons test, by Kruskal-Wallis non parametric test, and by Student's t-test where appropriate. Analyses were performed using Graph-Pad Prism Version 8.0.2 (GraphPad Software, https://www.graphpad.com) with statistical significance set at *p < 0.05. For proteomic analysis, the quantification data obtained from Spectronaut (Protein Quant Pivot Report) was imported into Perseus software version 1.6.15.0 [33]. To ensure data quality, protein groups with less than 70 % valid intensity values were filtered out. The raw intensities were then log2-transformed and normalized using quantile normalization to account for technical variations. Missing values were imputed with random numbers drawn from a normal distribution to simulate low abundance values close to noise levels. The quantified proteome was divided into five quantiles based on the median abundance of each protein. Enrichment analysis was performed on the most abundant proteins (top 5th quantile) using ShinyGO v0.80 [34] with statistical significance set at FDR <0.05 for biological processes and cellular components.

3. Results

3.1. hAF is enriched with small EVs with heterogeneous phenotype

hAF samples were processed by SEC followed by concentration of EVs by ultracentrifugation (Suppl Fig. 1A); hAF-EV yield was 6.31 ± 0.98 × 10^9 particles/hAF ml (Suppl Fig. 1B); EVs showed canonical round cup-shaped morphology and 209.63 ± 6.10 nm and 125.99 ± 54.31 nm average size by NTA and TEM analyses (Fig. 1A–B). hAF-EVs were found positive for the CD9, CD63 and CD81 tetraspanin signature (Fig. 1C–D). Expression of Syntenin-1, TSG101, and ALIX markers by WB further confirmed the enrichment of small EVs in the preparations with concomitant lack of ApoB-positive lipoprotein cross-contamination (Fig. 1D). hAF-EV phenotypic profile by MACSPlex assay showed a positive trend of enrichment for CD133/1, CD326, CD24, CD29 and SSEA4 (Fig. 1E). Single particle analysis by super-resolution microscopy indicated 26.61 ± 5.26 % of small hAF-EVs co-expressing HLA-G on their surface, alongside CD9 and CD63 (Fig. 1F).

3.2. hAF-EVs antagonise oxidative stress on target cells

C2C12 viability was significantly affected by H_2O_2 injury, as decreasing to 71.79 ± 3.08 % compared to control cells treated with vehicle solution (****p < 0.0001); hAF-EV stimulation did not alter cells in standard condition, while their priming before oxidative injury resulted in relevant rescue of viability up to 91.29 ± 12.84 % (*p < 0.05, Fig. 2A). Fluorescently DiR-labelled hAF-EVs (DiR + hAF-EVs) were uptaken by target C2C12 cells as analysed after 24 h incubation (Fig. 2B). C2C12 exposed to H_2O_2 stress presented metabolic alteration with impaired ATP synthesis and OCR with enhanced lactate dehydrogenase (LDH) activity and increased malondialdehyde accumulation (****p < 0.0001). hAF-EVs priming appreciably counteracted such signs of metabolic dysfunction (****p < 0.0001, Fig. 2C). A human 3D cardiac microtissue (hMT, [35]) culture system was also employed as in vitro preclinical model of cardiac oxidative stress. hMT were affected by oxidative stress as assessed by CCK8 assay, with hAF-EVs pre-treatment significantly rescuing their viability (****p < 0.0001, Fig. 2D). Immunostaining analysis for C-Casp3 further confirmed a relevant 2-fold increased expression (*p < 0.05) in hMT undergoing oxidative injury, while hAF-EVs stimulation promptly reduced the activation of cell death program to physiological levels (**p < 0.01, Fig. 2D). DiR + hAF-EVs were uptaken by target hMT as analysed after 24 h incubation (Fig. 2E).

3.3. hAF-EVs prevent the pro-fibrotic commitment of target cells

H_2O_2-induced activation of cardiac fibroblast into pro-fibrotic myofibroblast in hMT was detected by a 2-fold increased expression of Collagen I mRNA; such effect was tamed down by hAF-EVs (*p < 0.05, Fig. 3A). We further confirmed that reactive oxygen species (ROS, detected by DHE) are released by hCF undergoing TGFβ stimulation for 3 h (*p < 0.05, Fig. 3B). We translated this finding to our 3D hMT model; hMT exposed to TGFβ over 7 days were remarkably smaller (****p < 0.0001), in agreement to Ref. [36]; treatment with hAF-EVs showed a trend in preventing their size condensation (Fig. 3C). TGFβ-stimulated hMT also presented a significant 1.8- and 2.5-fold increase of Vimentin- and αSMA-positive hCF over cTnT-positive cardiomyocytes, respectively (**p < 0.01, Fig. 3D; *p < 0.05, Fig. 3E). hMT receiving hAF-EVs showed substantial reduction of Vimentin-positive and αSMA-positive cells over cTnT-positive ones (*p < 0.05 and ****p < 0.0001 respectively, Fig. 3D–E).

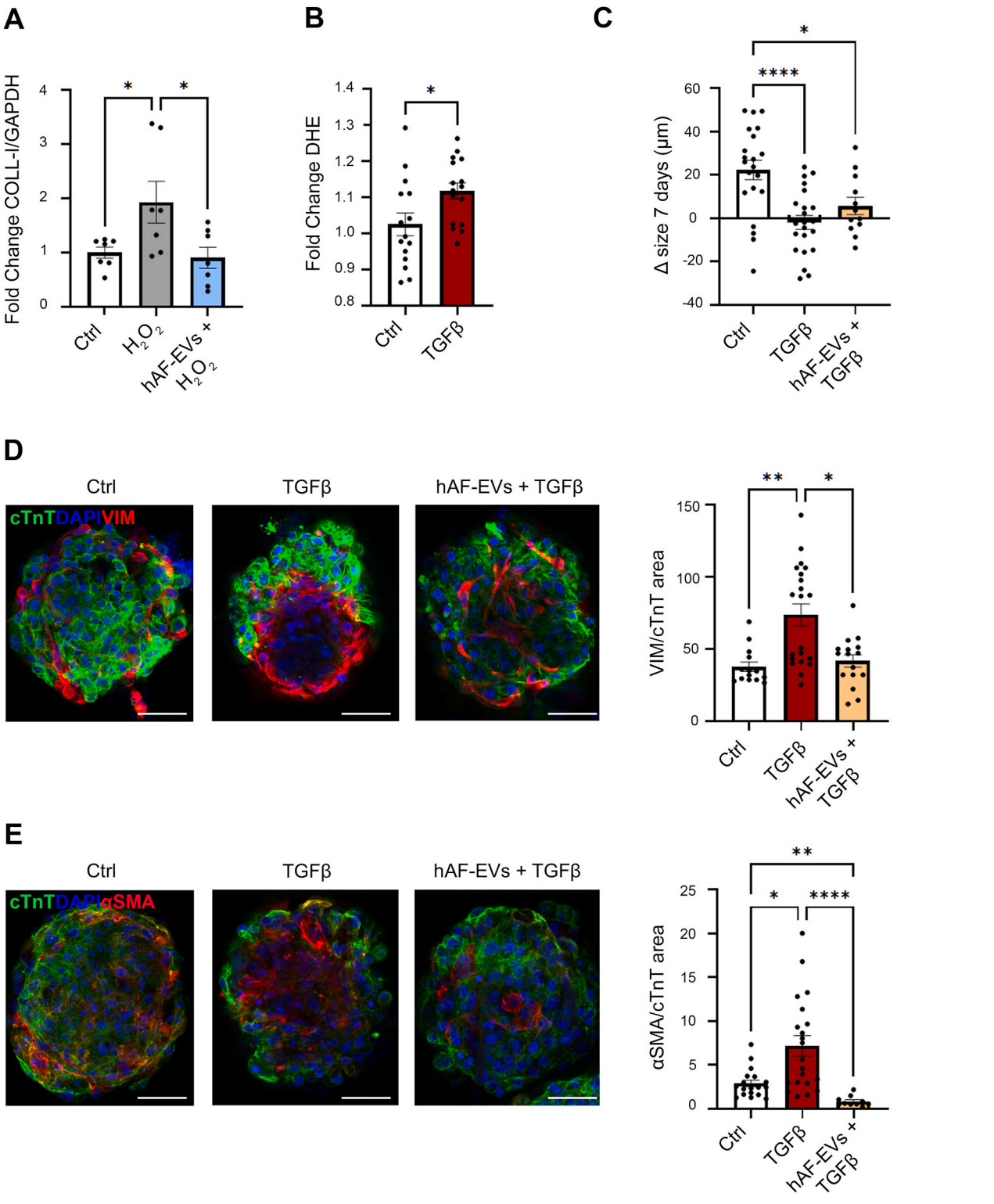

(caption on next page)

Fig. 3. hAF-EV paracrine potential against oxidative stress from pro-fibrotic activation. A) Real-time qRT-PCR analysis for Collagen 1 (COLL-1) expression over GAPDH as housekeeping. The graph shows the mean ± s.e.m fold change value of COLL-1/GAPDH of hMT with and without oxidative stress and hAF-EVs priming (n = 7; *Ctrl*: 1.00 ± 0.10; H_2O_2: 1.93 ± 0.39; *hAF-EVs* + H_2O_2: 0.91 ± 0.20; *p = 0.049 *Ctrl* versus H_2O_2; *p = 0.0292 H_2O_2 versus *hAF-EVs* + H_2O_2). **B)** Evaluation of ROS production by DHE assay on hCF with and without TGFβ treatment; the graph shows the mean ± s.e.m of fold change value (Ctrl: 1.02 ± 0.03, n = 15; TGFβ: 1.12 ± 0.02, n = 16; *p = 0.023). **C)** Evaluation of hMT size variation (Δ size in μm) cultured in control conditions (*Ctrl*), with TGFβ treatment (*TGFβ*) and with hAF-EV and TGFβ treatment (*hAF-EVs* + *TGFβ*) after 7 days (*Ctrl*: 22.30 ± 4.50, n = 21; *TGFβ*: −1.93 ± 3.20, n = 22; *hAF-EVs* + *TGFβ*: 5.63 ± 4.00, n = 13; ****p < 0.0001; *p = 0.0256; *μm: micron*). **D)** Immunohistochemical staining for Vimentin (VIM) over cardiac Troponin T (cTnT) expression within hMT cultured in control conditions (*Ctrl*), with TGFβ treatment (*TGFβ*) and with hAF-EV and TGFβ treatment (*hAF-EVs* + *TGFβ*); on the left: representative images showing cTnT-positive cardiomyocytes (green) and VIM-positive fibroblasts (red), nuclei are in blue by DAPI staining; scale bar: 50 μm; on the right, the graph shows the mean ± s.e.m of VIM/cTnT area in arbitrary units (*Ctrl*: 37.74 ± 3.36, n = 14; *TGFβ*: 73.68 ± 7.51, n = 21; *hAF-EVs* + *TGFβ*: 41.77 ± 4.35, n = 16; **p = 0.002; *p = 0.0476). **E)** Immunohistochemical staining for alpha smooth muscle actin (aSMA) over cardiac Troponin T (cTnT) expression within hMT cultured in control conditions (*Ctrl*), with TGFβ treatment (*TGFβ*) and with hAF-EV and TGFβ treatment (*hAF-EVs* + *TGFβ*); on the left: representative images showing cTnT-positive cardiomyocytes (green) and aSMA-positive myofibroblasts (red), nuclei are in blue by DAPI staining; scale bar: 50 μm; on the right, the graph shows the mean ± s.e.m of aSMA/cTnT area in arbitrary units (*Ctrl*: 2.90 ± 0.39, n = 18; *TGFβ*: 7.20 ± 1.20, n = 21; *hAF-EVs* + *TGFβ*: 0.80 ± 0.18, n = 10; *p = 0.0498; **p = 0.0085; ****p < 0.0001). (For interpretation of the references to colour in this figure legend, the reader is referred to the Web version of this article.)

3.4. *hAF-EVs are enriched with functional molecular cargo*

The identified proteins within hAF-EV cargo (n = 3351) were divided into 5 quantiles (Q1-5, Fig. 4A); biological process and cellular component gene ontology (GO) analyses of the 670 more expressed in Q5 suggested the presence of proteins involved in extracellular vesicle organization and transport (Supplementary Fig. 2), confirming EV identity. We also appreciated the presence of proteins related to different pathways involved in energetic metabolism (glycolysis, Krebs cycle, oxidative phosphorylation) and antioxidant response (glutathione metabolism, catalase, superoxide dismutase pathway, peroxiredoxin family, Fig. 4B and Table 1), thus suggesting EV protective role against oxidative stress. MSC-EVs have been previously shown to conduct aerobic metabolism [30,37]. Likewise, hAF-EVs undergoing OxPhos evaluation presented *de novo* ATP synthesis and oxygen consumption (Fig. 4C). Whole-transcriptome RNAseq analysis of hAF-EVs resulted in a total of 8558 RNA species with TPMs >1. We then performed enrichment analysis of the 633 transcripts with a TPMs level higher than total transcript median average (18.37 TPM). GO enrichment analysis for biological processes highlighted the presence of RNA species involved in ATP biosynthesis (Fig. 4D); GO for molecular function identified genes involved in the oxidoreduction-driven active transmembrane transporter activity (Fig. 4E), and KEGG analysis confirmed these data suggesting the presence of RNA involved in the oxidative phosphorylation (Fig. 4F and Table 2). This analysis also allowed the identification of different transcripts belonging to ribosomal constituents, in addition to few ribonucleoproteins.

4. Discussion

We previously characterised the paracrine therapeutic profile of secretome fractions from hAFSC obtained from leftover and clinical waste samples of hAF from II and III trimester of gestation. Immature hAFSC obtained from prenatal screening via routine amniocentesis procedure can exert relevant cardio-active effects by secreting pro-resolving and anti-aging EVs [8,38]. Nonetheless, the separation and concentration of secretome components from hAFSC require prolonged in vitro cell expansion and different steps for EV processing. Here we focused on profiling EVs directly concentrated from leftover samples of II trimester hAF as starting material, to assess their paracrine potential and whether they can offer a relevant alternative.

The hAF is a complex biofluid and it becomes enriched with heterogeneous metabolites during gestation [39,40] hAF composition reflects the changes during pregnancy, especially during the III trimester, due to the contribution of fetal urine and pulmonary, cardiovascular, renal, and endothelial secretions [41]. hAF-EVs represent a heterogeneous population from different contributions: placenta membranes, cells present in the amniotic fluid (including hAFSC), and cells deriving from the fetal pulmonary and gastrointestinal tract. The first evidence of hAF-EVs as diagnostic elements comes from a study in 2017 showing the procoagulant capacity of phosphatidylserine- and tissue factor-enriched hAF-EVs during amniotic fluid embolism driving disseminated intravascular coagulation [42]. Small EVs from hAF have been shown to act as informative biomarkers for antenatal hydronephrosis diagnosis, according to their moesin content [43] and to be dysregulated in their microRNA (miRNA) components in fetuses with congenital diaphragmatic hernia [44]. Likewise, III trimester hAF-EVs have been found functionally related to preeclampsia by means of increased expression of CD105 (endoglin), which may concur to anti-angiogenic effects [28].

To the best of our knowledge, here we present first-time evidence that II trimester hAF is enriched with EVs with paracrine potential in antagonising oxidative stress on target cells. By optimising EV separation from hAF, we obtain a relevantly high particle yield with canonical EV morphology and dimension. While we cannot identify a unique origin for II trimester hAF-EVs, we found a positive trend of the enrichment for CD133/1, CD326, CD24, CD29 and SSEA4 antigens in their phenotypic signature, implying a contribution from amniotic fluid and fetal urine [28], as well as by immature stem cells [45], including hAFSC [7]. Compared to III trimester hAF-EVs, our EVs showed limited placental inception as by HLA-G expression [28], thus suggesting fetal origin with less committed potential.

We have demonstrated that hAFSC secretome components, including hAFSC-EVs, are remarkably active in counteracting oxidative stress and exacerbation of fibrosis on cardiac cells and the myocardial tissue in preclinical models of disease [12,46]; here we investigated whether II trimester hAF-EVs may exert similar effects. II trimester hAF-EVs exerted cytoprotective potential on murine myoblasts exposed to H_2O_2 injury, similarly to what we initially reported for hAFSC-EVs on the same cell line in vitro [7], by means of metabolic rescue based on supporting ATP production and limiting activation of intracellular oxidative pathways. We confirmed these results on a human cardiac microtissue model, with relevant hAF-EVs trophic potential in preserving cell viability and counteracting oxidative injury, a hallmark of cardiac dysfunction. Notably, another read-out of cardiac injury triggered by oxidative stress is the commitment of fibroblasts into pro-fibrotic myofibroblasts [47]; myofibroblasts produce extracellular matrix components leading to fibrosis development and resulting into extensive scarring [48]. We confirmed that hAF-EVs can protect hMT against H_2O_2-dependent fibroblast activation as early as within the first 24 h. Moreover, myofibroblast activation by TGFβ stimulation is a well-known pathway [49] with one of the TGFβ-activated cascades being the oxidative stress [50]; in our 3D cardiac model of oxidative-related fibrosis, hAF-EVs promptly quenched the expansion of activated myofibroblasts to the detriment of the cardiomyocyte counterpart. Overall, this data suggests a therapeutically relevant paracrine role of hAF-EVs against the scarring process, possibly through prevention of oxidative stress induction.

hAF-EVs were also found expressing aerobic respiratory capacity, although with limited OxPhos efficiency; this may indicate that immature and "developmentally juvenile" EVs from early-mid gestation

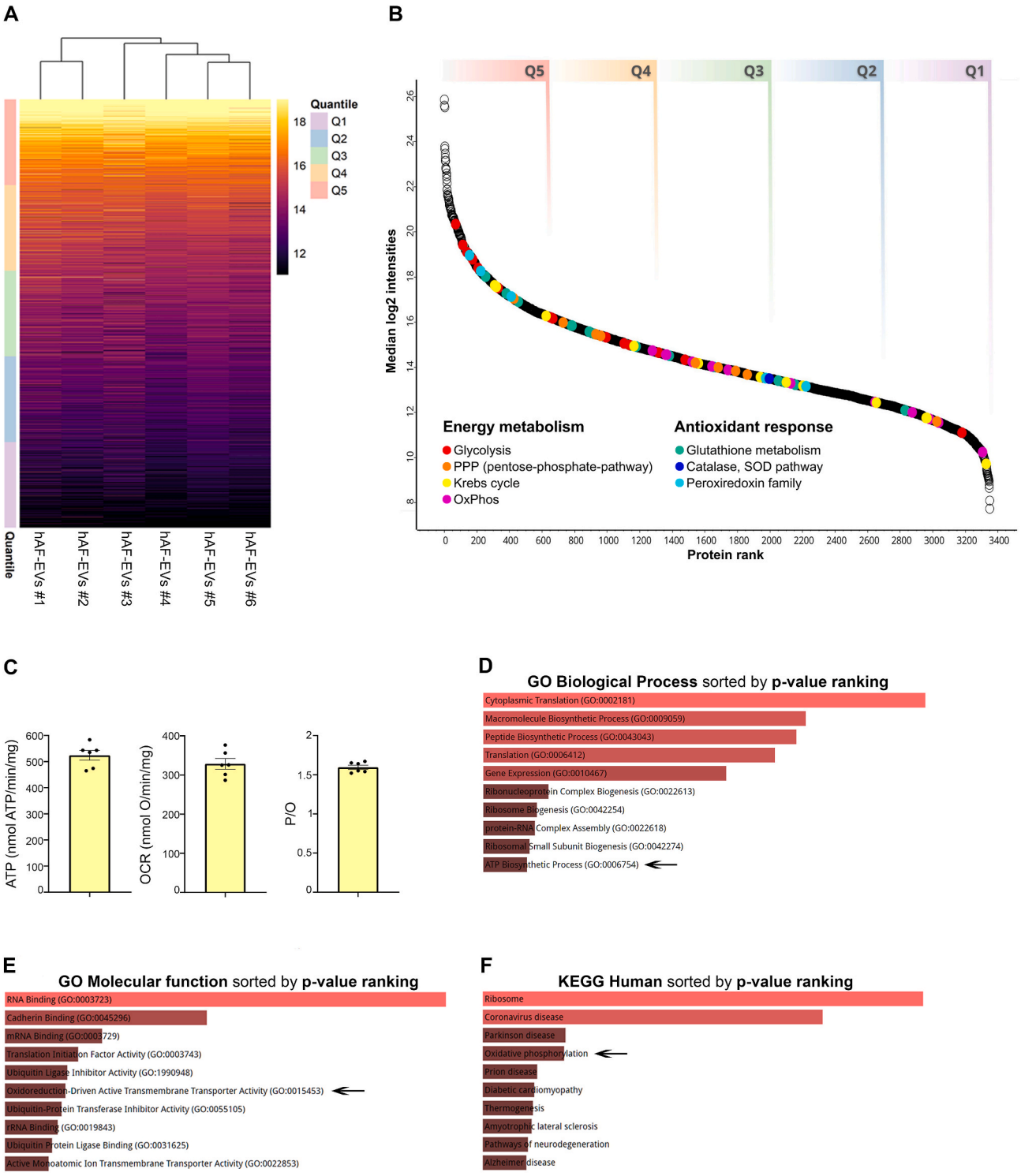

Fig. 4. Characterization of hAF-EV cargo. A) Heatmap of protein expression levels in hAF-EV samples (n = 6). The 3351 identified proteins are divided into five quantiles (Q1-Q5) based on their median log2 intensity, with Q1 representing the lowest and Q5 representing the highest values. **B)** Rank plot showing proteins detected in hAF-EVs (x-axis) ranked from highest to lowest median log2 protein abundance (y-axis). Proteins related to energy metabolism and antioxidant response are highlighted. **C)** Metabolic profile of hAF-EV samples (n = 6) in terms of ATP synthesis (523.97 ± 18.64 nmol ATP/min/mg), OCR (328.61 ± 13.63 nmol O/min/mg) and P/O (1.60 ± 0.03). **D-F)** Enrichment analysis from RNAseq of hAF-EV samples (n = 7) with enrichment analysis for GO biological process, GO molecular function and KEGG human gene ontology sorted by p-value ranking; arrows pointing at ATP biosynthetic process, oxidoreduction-driven active transmembrane transporter activity and oxidative phosphorylation. *GO: gene ontology; Q: quantile; SOD: superoxide dismutase; OxPhos: oxidative phosphorylation; nmol: nanomoles; min: minutes; mg: milligrams; O: oxygen; KEGG: Kyoto encyclopaedia of genes and genomes.*

Table 1
List of proteins involved in different pathways involved in energetic metabolism and antioxidant response as identified within hAF-EVs by proteomic analysis.

Glycolysis	PPP	Krebs Cycle	OxPhos	Glutatione metabolism	Catalase, SOD Pathway	Peroxiredoxin family
GAPDH	PGD	IDH1	SDHB	GSTP1	CAT	PRDX6
PKM	TALDO1	MDH1	CYB5R3	GSTO1	SOD1	PRDX2
ENO1	TKT	ACO1	CYB5R2	LANCL1		PRDX5
PGK1	PGLS	DLST	ATP5F1B	GSTA2		TXNL1
TPI1	RBKS	ACO2	ATP5F1A	GPX3		PXDN
ALDOA	DERA	SUCLG2	CYB561	GSR		
PGAM1	SHPK	MDH2	ETFB	GSS		
GPI	G6PD	CS	ETFA	GSTM2		
ALDOB	RPIA	IDH2	NDUFA6	GSTT1		
PKLR		PDHB	COX7A2	GSTM1		
PFKP		FH	NDUFV1	HAGH		
ALDOC		SLC25A1	MT-CO2	MGST2		
PFKL		SUCLG1	NDUFS2	GSTM3		
BPGM		IDH3G	SDHA	GPX1		
PFKM		IDH3A	ATP5PO	GCLC		
TIGAR			NDUFS3	GSTA4		
HKDC1			UQCR10	GGT7		
			NDUFB10	GSTK1		
			ATP5MC1	ABCC1		
			SDHB	GSTT2		
				GSTCD		
				MGST3		
				GSTM4		
				GSTP1		

Table 2
List of genes identified by enrichment analysis for biological process, molecular function and KEGG human gene ontology in the hAF-EV cargo by RNA sequencing.

ATP Biosyntetic Process (GO:0006754)	Oxidoreduction-Driven Active Transmembrane Transporter Activity (GO:0015453)	Oxidative Phosporylation
ATP5ME	COX7C	COX7C
ALDOA	COX4I1	ATP5ME
ATP5MC2	UQCRH	COX4I1
ATP5MG	NDUFS5	ATP5MC2
ATP5MK	UQCRB	UQCRH
ATP5MF	COX6B1	ATP5MG
ATP5PO	COX8A	UQCRQ
ATP5PD	NDUFB10	NDUFS5
ATP5F1A	NDUFA3	UQCRB
ATP5F1D	COX5A	COX6B1
ATP5F1C	NDUFB2	COX8A
ATP5MJ	NDUFA1	ATP6V1F
ATP5F1B	UQCR10	ATP5MF
ATP5PF	COX5B	ATP5PO
	NDUFB4	ATP5PD
		COX7A2
		NDUFB10
		NDUFA13
		ATP5F1A
		NDUFA3
		COX6C
		ATP5F1D
		COX5A
		NDUFB2
		ATP6V0C
		NDUFA1
		UQCR10
		ATP5F1C
		COX5B
		ATP5F1B
		COX6A1
		NDUFB4
		ATP5PF

amniotic fluid may present significant potential in rescuing cell bioenergetics, thus counteracting oxidative stress leading to *inflammaging*. While previous studies indicated that human umbilical cord-MSC-EVs can express the respiratory complexes I, IV, and V able to conduct the OxPhos metabolism, functional ATP synthesis was detected only in EVs released from MSC obtained by term perinatal derivatives, hence indicating that gestational stage may impact on aerobic metabolism potential [30]. II trimester hAF-EVs seem not to be affected by any requirement for gestational maturation, thus representing candidate therapeutics to improve the energy metabolism of the injured cells. Indeed, hAF-EV characterization by proteomics and RNA sequencing further suggested a healing role against oxidative stress, with their cargo including components related to energetic metabolism, antioxidant response pathways, ATP synthesis, oxidoreduction-driven transmembrane transporter activity and OxPhos. Notably, While the hAF-EV morphological features are comparable to those of their cellular counterpart (as for II trimester hAFSC-EVs), we have appreciated a different proteomic profile. The II trimester hAFSC-EV proteome content that we previously characterized is enriched with molecular mediators involved in cardiovascular development, vascular remodelling and myocardial renewal, thus supporting their relevant cardioactive and cardioprotective paracrine role [38]. Here, the proteomic analysis of the hAF-EV cargo indicates protein elements involved in EV organization and transport along with mediators that may be involved in energetic metabolism signalling. While hAFSC-EVs may represent a more homogeneous population as obtained by in vitro cell culture and by hAFSC-conditioned medium as staring material, hAF-EV preparations may be enriched in vesicles secreted into the amniotic fluid by different cell sources (amniotic membrane progenitors, hAFSC in the amniotic fluid, fetal cells, etc.). Thus, their cargo may be more heterogeneous.

Recently, a few studies on the pro-regenerative angiogenic and anti-inflammatory potential of hAF-EVs separated from III trimester/term amniotic fluid obtained during scheduled C-section delivery procedures have been also reported [21,22,24]. From a translational perspective, III trimester hAF may offer a feasible source of EVs as future theranostic tools. Further analyses to provide a direct comparison of the paracrine effects of more immature II trimester hAF-EVs versus the perinatal III trimester ones are required to identify the source with the most relevant paracrine potential for different therapeutic applications according to the specific disease.

4.1. Conclusions

In this study we characterised EVs obtained by a straightforward protocol from leftover samples of early-mid gestation hAF from prenatal

screening. hAF-EVs were able to improve the bioenergetics of injured cells via paracrine effects. These findings may support hAF-EVs as future candidate therapeutics against inflammatory-based dysfunction affecting the skeletal and cardiac muscle. Additional experiments are required to pinpoint the EV functional mechanism(s) of action by targeting molecular candidates within their cargo and to consolidate our findings in other relevant preclinical models of inflammation-related disease.

Supplementary Material

Supplementary Figuresare available in the Supplementary Material.

Ethics approval

All procedures were performed in compliance with relevant laws and institutional guidelines and have been approved by the appropriate institutional committee. The work described in this study has been carried out in compliance with the guidelines of the Declaration of Helsinki for the use of leftover and clinical waste samples of human amniotic fluid and human adult cardiac tissue as approved by the Regional Ethic Committees (*Comitato Etico Regionale Liguria* ref. P.R. 428REG2015 and *Comitato Etico Cantonale,* Bellinzona, Switzerland ref. CE 2923). Samples of human amniotic fluid and atrial specimens were obtained following written informed consent from donors. The patients/participants provided their written informed consent to donate the tissue for research purposes.

CRediT authorship contribution statement

Senesi Giorgia: Writing – original draft, Methodology, Investigation, Data curation. **Guerricchio Laura:** Writing – original draft, Methodology, Investigation, Data curation. **Ghelardoni Maddalena:** Writing – original draft, Methodology, Investigation, Data curation. **Bertola Nadia:** Formal analysis. **Rebellato Stefano:** Formal analysis. **Grinovero Nicole:** Data curation. **Bartolucci Martina:** Formal analysis. **Costa Ambra:** Methodology. **Raimondi Andrea:** Formal analysis. **Grange Cristina:** Formal analysis. **Bolis Sara:** Formal analysis. **Massa Valentina:** Formal analysis. **Paladini Dario:** Resources. **Coviello Domenico:** Resources. **Pandolfi Assunta:** Resources. **Bussolati Benedetta:** Resources. **Petretto Andrea:** Supervision, Data curation. **Fazio Grazia:** Supervision, Data curation. **Ravera Silvia:** Supervision, Data curation. **Barile Lucio:** Resources. **Balbi Carolina:** Writing – review & editing, Supervision, Project administration, Conceptualization. **Bollini Sveva:** Writing – review & editing, Supervision, Project administration, Conceptualization.

Declaration of competing interest

The authors have nothing to disclose nor competing interests to declare.

Data availability

Data will be made available on request.

Acknowledgements

The Authors thank all the other members of their laboratory for their insight and technical support. Bertola N. N.B. has been supported by the Italian Ministry of Health (*Ricerca Corrente*) and the Italian Ministry of Health 5 × 1000 funds 2021. Rebellato S. is a fellow of the University of Milano-Bicocca, Milan, Doctoral Program in Molecular and Translational Medicine (DIMET). Prof. Lucio Barile obtained financial support from Swiss National Foundation, SINERGIA grant number 202302 and Gustav & Ruth Jacob Foundation, Lugano, (2023). This research did not receive any specific grant from funding agencies in the public, commercial, or not-for-profit sectors.

Appendix A. Supplementary data

Supplementary data to this article can be found online at https://doi.org/10.1016/j.redox.2024.103241.

References

[1] M. Pozzobon, S. D'Agostino, M.G. Roubelakis, A. Cargnoni, R. Gramignoli, S. Wolbank, F. Gindraux, S. Bollini, H. Kerdjoudj, M. Fenelon, R. Di Pietro, M. Basile, V. Borutinskaite, R. Piva, A. Schoeberlein, G. Eissner, B. Giebel, P. Ponsaert, General consensus on multimodal functions and validation analysis of perinatal derivatives for regenerative medicine applications, Front. Bioeng. Biotechnol. 10 (2022) 961987, https://doi.org/10.3389/fbioe.2022.961987.

[2] A.R. Silini, R. Di Pietro, I. Lang-Olip, F. Alviano, A. Banerjee, M. Basile, V. Borutinskaite, G. Eissner, A. Gellhaus, B. Giebel, Y. Huang, A. Janev, M. Erdani Kreft, N. Kupper, A.C. Abadia-Molina, E.G. Olivares, A. Pandolfi, A. Papait, M. Pozzobon, C. Ruiz-Ruiz, O. Soritau, S. Susman, D. Szukiewicz, A. Weidinger, S. Wolbank, B. Huppertz, O. Parolini, Perinatal derivatives: where do we stand? A roadmap of the human placenta and consensus for tissue and cell nomenclature, Front. Bioeng. Biotechnol. 8 (2020) 610544, https://doi.org/10.3389/fbioe.2020.610544.

[3] A. Papait, A.R. Silini, M. Gazouli, R. Malvicini, M. Muraca, L. O'Driscoll, N. Pacienza, W.S. Toh, G. Yannarelli, P. Ponsaerts, O. Parolini, G. Eissner, M. Pozzobon, S.K. Lim, B. Giebel, Perinatal derivatives: how to best validate their immunomodulatory functions, Front. Bioeng. Biotechnol. 10 (2022) 981061, https://doi.org/10.3389/fbioe.2022.981061.

[4] S. Bollini, K.K. Cheung, J. Riegler, X. Dong, N. Smart, M. Ghionzoli, S. P. Loukogeorgakis, P. Maghsoudlou, K.N. Dube, P.R. Riley, M.F. Lythgoe, P. De Coppi, Amniotic fluid stem cells are cardioprotective following acute myocardial infarction, Stem Cell. Dev. 20 (2011) 1985–1994, https://doi.org/10.1089/scd.2010.0424.

[5] A. Zani, M. Cananzi, F. Fascetti-Leon, G. Lauriti, V.V. Smith, S. Bollini, M. Ghionzoli, A. D'Arrigo, M. Pozzobon, M. Piccoli, A. Hicks, J. Wells, B. Siow, N. J. Sebire, C. Bishop, A. Leon, A. Atala, M.F. Lythgoe, A. Pierro, S. Eaton, P. De Coppi, Amniotic fluid stem cells improve survival and enhance repair of damaged intestine in necrotising enterocolitis via a COX-2 dependent mechanism, Gut 63 (2014) 300–309, https://doi.org/10.1136/gutjnl-2012-303735.

[6] E. Lazzarini, C. Balbi, P. Altieri, U. Pfeffer, E. Gambini, M. Canepa, L. Varesio, M. C. Bosco, D. Coviello, G. Pompilio, C. Brunelli, R. Cancedda, P. Ameri, S. Bollini, The human amniotic fluid stem cell secretome effectively counteracts doxorubicin-induced cardiotoxicity, Sci. Rep. 6 (2016) 29994, https://doi.org/10.1038/srep29994.

[7] C. Balbi, M. Piccoli, L. Barile, A. Papait, A. Armirotti, E. Principi, D. Reverberi, L. Pascucci, P. Becherini, L. Varesio, M. Mogni, D. Coviello, T. Bandiera, M. Pozzobon, R. Cancedda, S. Bollini, First characterization of human amniotic fluid stem cell extracellular vesicles as a powerful paracrine tool endowed with regenerative potential, Stem Cells Transl. Med. 6 (2017) 1340–1355, https://doi.org/10.1002/sctm.16-0297.

[8] A. Costa, C. Balbi, P. Garbati, M.E.F. Palama, D. Reverberi, A. De Palma, R. Rossi, D. Paladini, D. Coviello, P. De Biasio, D. Ceresa, P. Malatesta, P. Mauri, R. Quarto, C. Gentili, L. Barile, S. Bollini, Investigating the paracrine role of perinatal derivatives: human amniotic fluid stem cell-extracellular vesicles show promising transient potential for cardiomyocyte renewal, Front. Bioeng. Biotechnol. 10 (2022) 902038, https://doi.org/10.3389/fbioe.2022.902038.

[9] F. Villa, S. Bruno, A. Costa, M. Li, M. Russo, J. Cimino, P. Altieri, C. Ruggeri, C. Gorgun, P. De Biasio, D. Paladini, D. Coviello, R. Quarto, P. Ameri, A. Ghigo, S. Ravera, R. Tasso, S. Bollini, The human fetal and adult stem cell secretome can exert cardioprotective paracrine effects against cardiotoxicity and oxidative stress from cancer treatment, Cancers 13 (2021) 3729, https://doi.org/10.3390/cancers13153729.

[10] S. Sedrakyan, V. Villani, S. Da Sacco, N. Tripuraneni, S. Porta, A. Achena, M. Lavarreda-Pearce, A. Petrosyan, H. Soloyan, R.E.D. Filippo, B. Bussolati, L. Perin, Amniotic fluid stem cell-derived vesicles protect from VEGF-induced endothelial damage, Sci. Rep. 7 (2017) 16875, https://doi.org/10.1038/s41598-017-17061-2, 2.

[11] B. Mellows, R. Mitchell, M. Antonioli, O. Kretz, D. Chambers, M. Zeuner, B. Denecke, L. Musante, D.L. Ramachandra, F. Debacq-Chainiaux, H. Holthofer, B. Joch, S. Ray, D. Widera, A.L. David, T.B. Huber, J. Dengjel, P. De Coppi, K. Patel, Protein and molecular characterization of a clinically compliant amniotic fluid stem cell-derived extracellular vesicle fraction capable of accelerating muscle regeneration through enhancement of angiogenesis, Stem Cell. Dev. 26 (2017) 1316–1333, https://doi.org/10.1089/scd.2017.0089.

[12] C. Balbi, K. Lodder, A. Costa, S. Moimas, F. Moccia, T. van Herwaarden, V. Rosti, F. Campagnoli, A. Palmeri, P. De Biasio, F. Santini, M. Giacca, M.J. Goumans, L. Barile, A.M. Smits, S. Bollini, Reactivating endogenous mechanisms of cardiac regeneration via paracrine boosting using the human amniotic fluid stem cell secretome, Int. J. Cardiol. 287 (2019) 87–95, https://doi.org/10.1016/j.ijcard.2019.04.011.

[13] M. Gatti, M. Zavatti, F. Beretti, D. Giuliani, E. Vandini, A. Ottani, E. Bertucci, T. Maraldi, Oxidative stress in alzheimer's disease: in vitro therapeutic effect of

amniotic fluid stem cells extracellular vesicles, Oxid. Med. Cell. Longev. 2020 (2020) 2785343, https://doi.org/10.1155/2020/2785343.
[14] M. Zavatti, M. Gatti, F. Beretti, C. Palumbo, T. Maraldi, Exosomes derived from human amniotic fluid mesenchymal stem cells preserve microglia and neuron cells from aβ, Int. J. Mol. Sci. 23 (2022) 4967, https://doi.org/10.3390/ijms23094967.
[15] L. Mezzasoma, I. Bellezza, P. Orvietani, G. Manni, M. Gargaro, K. Sagini, A. Llorente, P. Scarpelli, L. Pascucci, B. Cellini, V.N. Talesa, F. Fallarino, R. Romani, Amniotic fluid stem cell-derived extracellular vesicles are independent metabolic units capable of modulating inflammasome activation in THP-1 cells, Faseb. J. 36 (2022) e22218, https://doi.org/10.1096/fj.202101657R.
[16] M. Gatti, F. Beretti, M. Zavatti, E. Bertucci, S. Ribeiro Luz, C. Palumbo, T. Maraldi, Amniotic fluid stem cell-derived extracellular vesicles counteract steroid-induced osteoporosis in vitro, Int. J. Mol. Sci. 22 (2020) 38, https://doi.org/10.3390/ijms22010038.
[17] B. Li, C. Lee, J.S. O'Connell, L. Antounians, N. Ganji, M. Alganabi, M. Cadete, F. Nascimben, Y. Koike, A. Hock, S.R. Botts, R.Y. Wu, H. Miyake, A. Minich, A. F. Maalouf, E. Zani-Ruttenstock, Y. Chen, K.C. Johnson-Henry, P. De Coppi, S. Eaton, P. Maattanen, P. Delgado Olguin, A. Zani, P.M. Sherman, A. Pierro, Activation of wnt signaling by amniotic fluid stem cell-derived extracellular vesicles attenuates intestinal injury in experimental necrotizing enterocolitis, Cell Death Dis. 11 (2020) 750–752, https://doi.org/10.1038/s41419-020-02964-2.
[18] L. Antounians, V.D. Catania, L. Montalva, B.D. Liu, H. Hou, C. Chan, A.C. Matei, A. Tzanetakis, B. Li, R.L. Figueira, K.M. da Costa, A.P. Wong, R. Mitchell, A. L. David, K. Patel, P. De Coppi, L. Sbragia, M.D. Wilson, J. Rossant, A. Zani, Fetal lung underdevelopment is rescued by administration of amniotic fluid stem cell extracellular vesicles in rodents, Sci. Transl. Med. 13 (2021) eaax5941, https://doi.org/10.1126/scitranslmed.aax5941.
[19] A. Costa, R. Quarto, S. Bollini, Small extracellular vesicles from human amniotic fluid samples as promising theranostics, Int. J. Mol. Sci. 23 (2022) 590, https://doi.org/10.3390/ijms23020590.
[20] J.A. Welsh, D.C.I. Goberdhan, L. O'Driscoll, E.I. Buzas, C. Blenkiron, B. Bussolati, H. Cai, D. Di Vizio, T.A.P. Driedonks, U. Erdbrugger, J.M. Falcon-Perez, Q.L. Fu, A. F. Hill, M. Lenassi, S.K. Lim, M.G. Mahoney, S. Mohanty, A. Möller, R. Nieuwland, T. Ochiya, S. Sahoo, A.C. Torrecilhas, L. Zheng, A. Zijlstra, S. Abuelreich, R. Bagabas, P. Bergese, E.M. Bridges, M. Brucale, D. Burger, R.P. Carney, E. Cocucci, R. Crescitelli, E. Hanser, A.L. Harris, N.J. Haughey, A. Hendrix, A. R. Ivanov, T. Jovanovic-Talisman, N.A. Kruh-Garcia, V. Ku'ulei-Lyn Faustino, D. Kyburz, C. Lässer, K.M. Lennon, J. Lötvall, A.L. Maddox, E.S. Martens-Uzunova, R.R. Mizenko, L.A. Newman, A. Ridolfi, E. Rohde, T. Rojalin, A. Rowland, A. Saftics, U.S. Sandau, J.A. Saugstad, F. Shekari, S. Swift, D. Ter-Ovanesyan, J. P. Tosar, Z. Useckaite, F. Valle, Z. Varga, E. van der Pol, M.J.C. van Herwijnen, M. H.M. Wauben, A.M. Wehman, S. Williams, A. Zendrini, A.J. Zimmerman, M.I.S.E. V. Consortium, C. Théry, K.W. Witwer, Minimal information for studies of extracellular vesicles (MISEV2023): from basic to advanced approaches, J. Extracell. Vesicles 13 (2024) e12404, https://doi.org/10.1002/jev2.12404.
[21] P. Li, X. Lu, J. Hu, M. Dai, J. Yan, H. Tan, P. Yu, X. Chen, C. Zhang, Human amniotic fluid derived-exosomes alleviate hypoxic encephalopathy by enhancing angiogenesis in neonatal mice after hypoxia, Neurosci. Lett. 768 (2022) 136361, https://doi.org/10.1016/j.neulet.2021.136361.
[22] T. Del Rivero, J. Milberg, C. Bennett, M.I. Mitrani, M.A. Bellio, Human amniotic fluid derived extracellular vesicles attenuate T cell immune response, Front. Immunol. 13 (2022) 977809, https://doi.org/10.3389/fimmu.2022.977809.
[23] E. Nunzi, L. Mezzasoma, I. Bellezza, T. Zelante, P. Orvietani, G. Coata, I. Giardina, K. Sagini, G. Manni, A. Di Michele, M. Gargaro, V.N. Talesa, G. Di Rienzo, F. Fallarino, R. Romani, Microbiota-associated HAF-EVs regulate monocytes by triggering or inhibiting inflammasome activation, Int. J. Mol. Sci. 24 (2023) 2527, https://doi.org/10.3390/ijms24032527.
[24] D. Chanda, T. Del Rivero, R. Ghimire, S. More, M.I. Mitrani, M.A. Bellio, R. Channappanavar, Acellular human amniotic fluid-derived extracellular vesicles as novel anti-inflammatory therapeutics against SARS-CoV-2 infection, Viruses 16 (2024) 273, https://doi.org/10.3390/v16020273.
[25] C. Balbi, S. Bolis, G. Vassalli, L. Barile, Flow cytometric analysis of extracellular vesicles from cell-conditioned media, J. Vis. Exp. 144 (2019), https://doi.org/10.3791/59128.
[26] N. Koliha, Y. Wiencek, U. Heider, C. Jungst, N. Kladt, S. Krauthauser, I.C. D. Johnston, A. Bosio, A. Schauss, S. Wild, A novel multiplex bead-based platform highlights the diversity of extracellular vesicles, J. Extracell. Vesicles 5 (2016) 29975, https://doi.org/10.3402/jev.v5.29975.
[27] O.P.B. Wiklander, R.B. Bostancioglu, J.A. Welsh, A.M. Zickler, F. Murke, G. Corso, U. Felldin, D.W. Hagey, B. Evertsson, X. Liang, M.O. Gustafsson, D.K. Mohammad, C. Wiek, H. Hanenberg, M. Bremer, D. Gupta, M. Bjornstedt, B. Giebel, J.Z. Nordin, J.C. Jones, S. El Andaloussi, A. Gorgens, Systematic methodological evaluation of a multiplex bead-based flow cytometry assay for detection of extracellular vesicle surface signatures, Front. Immunol. 9 (2018) 1326, https://doi.org/10.3389/fimmu.2018.01326.
[28] N. Gebara, J. Scheel, R. Skovronova, C. Grange, L. Marozio, S. Gupta, V. Giorgione, F. Caicci, C. Benedetto, A. Khalil, B. Bussolati, Single extracellular vesicle analysis in human amniotic fluid shows evidence of phenotype alterations in preeclampsia, J. Extracell. Vesicles 11 (2022) e12217, https://doi.org/10.1002/jev2.12217.
[29] N.A. Kulak, G. Pichler, I. Paron, N. Nagaraj, M. Mann, Minimal, encapsulated proteomic-sample processing applied to copy-number estimation in eukaryotic cells, Nat. Methods 11 (2014) 319–324, https://doi.org/10.1038/nmeth.2834.
[30] I. Panfoli, S. Ravera, M. Podesta, C. Cossu, L. Santucci, M. Bartolucci, M. Bruschi, D. Calzia, F. Sabatini, M. Bruschettini, L.A. Ramenghi, O. Romantsik, D. Marimpietri, V. Pistoia, G. Ghiggeri, F. Frassoni, G. Candiano, Exosomes from human mesenchymal stem cells conduct aerobic metabolism in term and preterm newborn infants, Faseb. J. 30 (2016) 1416–1424, https://doi.org/10.1096/fj.15-279679.
[31] V. Lisi, G. Senesi, N. Bertola, M. Pecoraro, S. Bolis, A. Gualerzi, S. Picciolini, A. Raimondi, C. Fantini, E. Moretti, A. Parisi, P. Sgro, L. Di Luigi, R. Geiger, S. Ravera, G. Vassalli, D. Caporossi, C. Balbi, Plasma-derived extracellular vesicles released after endurance exercise exert cardioprotective activity through the activation of antioxidant pathways, Redox Biol. 63 (2023) 102737, https://doi.org/10.1016/j.redox.2023.102737.
[32] N. Bertola, P. Degan, E. Cappelli, S. Ravera, Mutated FANCA gene role in the modulation of energy metabolism and mitochondrial dynamics in head and neck squamous cell carcinoma, Cells 11 (2022) 2353, https://doi.org/10.3390/cells11152353.
[33] S. Tyanova, T. Temu, P. Sinitcyn, A. Carlson, M.Y. Hein, T. Geiger, M. Mann, J. Cox, The Perseus computational platform for comprehensive analysis of (Prote) Omics data, Nat. Methods 13 (2016) 731–740, https://doi.org/10.1038/nmeth.3901.
[34] S.X. Ge, D. Jung, R.ShinyGO. Yao, A graphical gene-set enrichment tool for animals and plants, Bioinformatics 36 (2020) 2628–2629, https://doi.org/10.1093/bioinformatics/btz931.
[35] G. Campostrini, V. Meraviglia, E. Giacomelli, R.W.J. van Helden, L. Yiangou, R. P. Davis, M. Bellin, V.V. Orlova, C.L. Generation Mummery, Functional analysis and applications of isogenic three-dimensional self-aggregating cardiac microtissues from human pluripotent stem cells, Nat. Protoc. 16 (2021) 2213–2256, https://doi.org/10.1038/s41596-021-00497-2.
[36] M. Lee, K.B. Jung, S. Jo, S. Hyun, K. Moon, J. Seo, S. Kim, M. Son, Modelling cardiac fibrosis using three-dimensional cardiac microtissues derived from human embryonic stem cells, J. Biol. Eng. 13 (2019) 15–16, https://doi.org/10.1186/s13036-019-0139-6, eCollection 2019.
[37] M. Bruschi, L. Santucci, S. Ravera, M. Bartolucci, A. Petretto, D. Calzia, G. M. Ghiggeri, L.A. Ramenghi, G. Candiano, I. Panfoli, Metabolic signature of microvesicles from umbilical cord mesenchymal stem cells of preterm and term infants, Proteonomics Clin. Appl. 12 (2018) e1700082, https://doi.org/10.1002/prca.201700082.
[38] A. Costa, D. Ceresa, A. De Palma, R. Rossi, S. Turturo, S. Santamaria, C. Balbi, F. Villa, D. Reverberi, K. Cortese, P. De Biasio, D. Paladini, D. Coviello, S. Ravera, P. Malatesta, P. Mauri, R. Quarto, S. Bollini, Comprehensive profiling of secretome formulations from fetal- and perinatal human amniotic fluid stem cells, Int. J. Mol. Sci. 22 (2021) 3713, https://doi.org/10.3390/ijms22073713.
[39] M.A. Underwood, W.M. Gilbert, M.P. Sherman, Amniotic fluid: not just fetal urine anymore, J. Perinatol. 25 (2005) 341–348, https://doi.org/10.1038/sj.jp.7211290.
[40] J. Suliburska, R. Kocylowski, I. Komorowicz, M. Grzesiak, P. Bogdanski, D. Baralkiewicz, Concentrations of mineral in amniotic fluid and their relations to selected maternal and fetal parameters, Biol. Trace Elem. Res. 172 (2016) 37–45, https://doi.org/10.1007/s12011-015-0557-3.
[41] C.M. Bowen, F.S. Ditmars, A. Gupta, J. Reems, W.S. Fagg, Cell-free amniotic fluid and regenerative medicine: current applications and future opportunities, Biomedicines 10 (2022) 2960, https://doi.org/10.3390/biomedicines10112960.
[42] L. Hell, L. Wisgrill, C. Ay, A. Spittler, M. Schwameis, B. Jilma, I. Pabinger, P. Altevogt, J. Thaler, Procoagulant extracellular vesicles in amniotic fluid, Transl. Res. 184 (2017) 12–20.e1, https://doi.org/10.1016/j.trsl.2017.01.003.
[43] J. Li, Y. Fu, Q. Liu, K. Shen, R. Yao, Y. Fu, Y. Lu, M. Xie, W. Jian, M. Guo, L. Dai, W. Zhang, Multiomics-based study of amniotic fluid small extracellular vesicles identified moesin as a biomarker for antenatal hydronephrosis, Clin. Transl. Med. 13 (2023) e1360, https://doi.org/10.1002/ctm2.1360.
[44] I. Fabietti, T. Nardi, C. Favero, L. Dioni, L. Cantone, L. Pergoli, M. Hoxha, E. Pinatel, F. Mosca, V. Bollati, N. Persico, Extracellular vesicles and their miRNA content in amniotic and tracheal fluids of fetuses with severe congenital diaphragmatic hernia undergoing fetal intervention, Cells 10 (2021) 1493, https://doi.org/10.3390/cells10061493.
[45] H. Wang, P. Gong, J. Li, Y. Fu, Z. Zhou, L. Liu, Role of CD133 in human embryonic stem cell proliferation and teratoma formation, Stem Cell Res. Ther. 11 (2020) 208, https://doi.org/10.1186/s13287-020-01729-0, 0.
[46] C. Balbi, K. Lodder, A. Costa, S. Moimas, F. Moccia, T. van Herwaarden, V. Rosti, F. Campagnoli, A. Palmeri, P. De Biasio, F. Santini, M. Giacca, M.J. Goumans, L. Barile, A.M. Smits, S. Bollini, Supporting data on in vitro cardioprotective and proliferative paracrine effects by the human amniotic fluid stem cell secretome, Data Brief 25 (2019) 104324, https://doi.org/10.1016/j.dib.2019.104324.
[47] P.K. Aujla, Z. Kassiri, Diverse origins and activation of fibroblasts in cardiac fibrosis, Cell. Signal. 78 (2021) 109869, https://doi.org/10.1016/j.cellsig.2020.109869.
[48] H. Kurose, Cardiac fibrosis and fibroblasts, Cells 10 (2021) 1716, https://doi.org/10.3390/cells10071716.
[49] A. TGFbeta Leask, Cardiac fibroblasts, and the fibrotic response, Cardiovasc. Res. 74 (2007) 207–212, https://doi.org/10.1016/j.cardiores.2006.07.012.
[50] R. Liu, K.A. Gaston Pravia, Oxidative stress and glutathione in TGF-beta-mediated fibrogenesis, Free Radic. Biol. Med. 48 (2010) 1–15, https://doi.org/10.1016/j.freeradbiomed.2009.09.026.